

## Space Weather

### RESEARCH ARTICLE

10.1029/2018SW001880

#### Key Points:

- This is the first study to link interplanetary shock impact angles and speeds to latitudinal generation of geomagnetically induced currents
- In general, high-speed and nearly frontal shocks are associated with identified high-risk GICs in all latitude regions
- High-risk GICs are observed in equatorial regions around 12 LT due to intensification of the EEJ current by high-speed, nearly frontal shocks

#### Supporting Information:

- Supporting Information S1
- Data Set S1

#### Correspondence to:

D. M. Oliveira,  
denny.m.deoliveira@nasa.gov

#### Citation:

Oliveira, D. M., Arel, D., Raeder, J., Zesta, E., Ngwira, C. M., Carter, B. A., et al. (2018). Geomagnetically induced currents caused by interplanetary shocks with different impact angles and speeds. *Space Weather*, 16, 636–647. <https://doi.org/10.1029/2018SW001880>

Received 3 APR 2018

Accepted 4 MAY 2018

Accepted article online 15 MAY 2018

Published online 15 JUN 2018

## Geomagnetically Induced Currents Caused by Interplanetary Shocks With Different Impact Angles and Speeds

D. M. Oliveira<sup>1,2</sup>, D. Arel<sup>3</sup>, J. Raeder<sup>3</sup>, E. Zesta<sup>2</sup>, C. M. Ngwira<sup>2,4</sup>, B. A. Carter<sup>5</sup>, E. Yizengaw<sup>6</sup>, A. J. Halford<sup>7</sup>, B. T. Tsurutani<sup>8</sup>, and J. W. Gjerloev<sup>9,10</sup>

<sup>1</sup>Goddard Planetary Heliophysics Institute, University of Maryland, Baltimore County, Baltimore, MD, USA, <sup>2</sup>NASA Goddard Space Flight Center, Greenbelt, MD, USA, <sup>3</sup>Department of Physics and EOS Space Science Center, University of New Hampshire, Durham, NH, USA, <sup>4</sup>Department of Physics, Catholic University of America, Washington, DC, USA, <sup>5</sup>SPACE Research Centre, RMIT University, Melbourne, Victoria, Australia, <sup>6</sup>Institute for Scientific Research, Boston College, Boston, MA, USA, <sup>7</sup>The Aerospace Corporation, Chantilly, VA, USA, <sup>8</sup>Jet Propulsion Laboratory, California Institute of Technology, Pasadena, CA, USA, <sup>9</sup>The Johns Hopkins University Applied Physics Laboratory, Laurel, MD, USA, <sup>10</sup>Birkeland Centre of Excellence, University of Bergen, Bergen, Norway

**Abstract** The occurrence of geomagnetically induced currents (GICs) poses serious threats to modern technological infrastructure. Large GICs result from sharp variations of the geomagnetic field ( $dB/dt$ ) caused by changes of large-scale magnetospheric and ionospheric currents. Intense  $dB/dt$  perturbations are known to occur often in high-latitude regions as a result of storm time substorms. Magnetospheric compressions usually caused by interplanetary shocks increase the magnetopause current leading to  $dB/dt$  perturbations more evident in midlatitude to low-latitude regions, while they increase the equatorial electrojet current leading to  $dB/dt$  perturbations in dayside equatorial regions. We investigate the effects of shock impact angles and speeds on the subsequent  $dB/dt$  perturbations with a database of 547 shocks observed at the L1 point. By adopting the threshold of  $dB/dt = 100$  nT/min, identified as a risk factor to power systems, we find that  $dB/dt$  generally surpasses this threshold when following impacts of high-speed and nearly frontal shocks in dayside high-latitude locations. The same trend occurs at lower latitudes and for all nightside events but with fewer high-risk events. Particularly, we found nine events in equatorial locations with  $dB/dt > 100$  nT/min. All events were caused by high-speed and nearly frontal shock impacts and were observed by stations located around noon local time. These high-risk perturbations were caused by sudden strong and symmetric magnetospheric compressions, more effectively intensifying the equatorial electrojet current, leading to sharp  $dB/dt$  perturbations. We suggest that these results may provide insights for GIC forecasting aiming at preventing degradation of power systems due to GICs.

**Plain Language Summary** The occurrence of geomagnetically induced currents (GICs) poses serious threats to modern technological infrastructure. GIC effects are usually known to be elevated during geomagnetic storms in regions of high latitudes. However, there has recently been some attention to GIC effects in equatorial regions given a high number of power grids arising in those regions. Such stations may be located right beneath a strong electric current flowing in the dayside ionosphere, named the equatorial electrojet current. In this paper, we study the effects of shock waves driven by solar disturbances on the Earth's magnetic field and the subsequent generation of GICs on the ground. We associate, for the first time, shock impact angles and speeds with the subsequent GIC generation. We find that stations located beneath the equatorial electrojet current are subject to high-risk GIC intensifications if high-speed and nearly frontal shocks strike the Earth when the station is located around noon local time. We then suggest that power plant operators use real-time existing shock forecasting services to take actions in a time window of 30–60 min when a shock with high speed and small impact angle is detected around 1 million kilometers from Earth toward the Sun.

### 1. Introduction

The Sun is a magnetically active star with disturbances that are frequently generated on its surface that propagate explosively away through the heliosphere. If the disturbance speed relative to the medium speed is larger than the medium magnetosonic speed, interplanetary (IP) shocks are driven ahead of the disturbance

(Burlaga, 1971). IP shocks take place in all solar cycle phases but are more numerous during solar maxima (see, e.g., Kilpua et al., 2015; Oliveira & Raeder, 2015). IP shock strengths are usually expressed by shock speeds or magnetosonic Mach numbers, defined as the ratio of the shock relative (to the local medium) speed to the local magnetosonic speed (Burlaga, 1971; Tsurutani & Lin, 1985). When IP shocks interact with the Earth's magnetosphere, disturbances are observed in geospace and on the ground. The most well-known effect is the positive sudden impulse ( $SI^+$ ), resulted from the magnetosphere compression and manifested as sharp increases in the horizontal component of the geomagnetic field anywhere on the Earth and expressed by global geomagnetic indices (Araki, 1994; Araki et al., 2004; Smith et al., 1986).

IP shocks travel in the heliosphere with different shock normal orientations. When they impact the Earth's magnetosphere, different levels of geomagnetic activity may follow. For example, Takeuchi et al. (2002) suggested that a highly inclined IP shock was the cause of a gradual increase in the horizontal component of the global geomagnetic field, instead of the sharp increase normally observed. Simulation (Guo et al., 2005) and statistical (Wang et al., 2006) studies showed that the more frontal an IP shock strikes the Earth, the shorter the storm sudden commencement (or  $SI^+$  in general) rise time (RT) will be.

More recently, Oliveira and Raeder (2014) showed through simulations that IP shocks that strike the Earth with small impact angles may trigger higher geomagnetic activity than those with large impact angles, even if the latter are stronger than the former. They attributed such results to the symmetric magnetosphere compression resulting from the frontal case. Such results were later confirmed with a statistical study by Oliveira and Raeder (2015), who showed that substorm activity as measured by an enhanced version of the  $AL$  index correlated well with shock impact angles. More specifically, they showed that for strong shocks, the smaller the impact angle, the larger the triggering of geomagnetic activity. Later, similar results were obtained by Oliveira et al. (2016) for enhancements of the nightside auroral power intensity following shock impacts on the magnetosphere. A comprehensive review of this subject has recently been provided by Oliveira and Samsonov (2018).

The interaction of IP shocks with the Earth's magnetosphere is also a direct cause of large changes in the electric fields within the magnetosphere-ionosphere system (Gonzalez et al., 1994). Such highly variable geospace electric fields generate electric currents on the ground, which in turn induce, according to Faraday's law of induction (Pirjola, 2000, 2002), electric fields that couple with artificial conductors, affecting the flow of electric currents in power systems, leading to equipment damage and disruption of power supplies (Albertson et al., 1993; Bolduc, 2002; Béland & Small, 2005; Gaunt & Coetzee, 2007; Gaunt, 2016; Kappenman, 2003, 2006; Marshall et al., 2012). Such currents are the well-known geomagnetically induced currents (GICs), whose manifestation corresponds to abrupt and strong temporal changes in the geomagnetic field on the ground ( $dB/dt$ ) (Viljanen, 1998). Given the importance of the potential serious and widespread problems associated with disruptions to power systems, GICs have been characterized as one of the top space weather hazards by the scientific community and policy makers. This constant and imminent threat has led to regulatory actions not only in the United States but also at an international level (see, e.g., Cassak et al., 2017; Jonas & McCarron, 2015; Knipp, 2015; Pulkkinen et al., 2017). GICs are also a very common subject for modeling studies whose goal corresponds to the improvement of GIC forecasting (Barbosa et al., 2015, 2017; Blake et al., 2016; Boteler & Pirjola, 2017; Ngwira et al., 2009; Pulkkinen, 2015; Torta et al., 2017; Zhang et al., 2015, 2016).

The economic impact of extreme space weather on technological infrastructure, with great contribution from GIC effects, has been studied in the context of global power system failures (see, e.g., Eastwood et al., 2017; National Research Council, 2008; Schulte in den Bäumen et al., 2014). In a worst case scenario, it is estimated that the daily U.S. economic loss associated with an extremely intense geomagnetic storm would be quite high (Oughton et al., 2017). However, an extreme event is not always the cause of significant power grid failures and component damage. Forbes and St. Cyr (2008) showed that real-time electricity market is affected by local geomagnetic field fluctuations. Schrijver et al. (2014) analyzed a 10-year period of insurance claims for industrial electrical equipment and concluded that their rates augmented substantially on geomagnetically active days. Therefore, the understanding of GIC generation and its consequent impact on power infrastructure is an important subject for space weather investigations.

Historically, most studies involving GIC effects on the ground focus on events with severe geomagnetic activity, or geomagnetic storms (Bolduc, 2002; Ngwira et al., 2013; Oliveira & Ngwira, 2017; Pulkkinen et al., 2005), with emphasis on regions poleward of  $60^\circ$  magnetic latitude (Piccinelli & Krausmann, 2018; Pulkkinen et al., 2005, 2012; Wik et al., 2008). For example, the collapse of the Hydro-Québec power system in North America

was caused by the geomagnetic storm of 13–14 March 1989 (Béland & Small, 2005; Bolduc, 2002). The black-out following that storm was associated with permanent damage to a transformer located in a New Jersey power plant, in the United States, caused by substorm-like events leading to a  $dB/dt$  peak of approximately  $\sim 480$  nT/min. In equatorward regions, GICs are associated with geomagnetic storms and  $SI^+$  events (Béland & Small, 2005; Carter et al., 2015; Fiori et al., 2014; Kappenman, 2003; Zhang et al., 2015, 2016; Zois, 2013). Zois (2013) showed that the number of reported transformer failures in a period of  $\sim 20$  years in midlatitude regions in Greece ( $35^\circ$ – $41^\circ$ ) was associated with solar activity. Zhang et al. (2015) showed that GIC response to the  $SI^+$  event preceding the 2015 St. Patrick's Day storm recorded by midlatitude stations along the Chinese coast was larger than those recorded at the same stations during storm main phase. Carter et al. (2016) reported that a South American equatorial station showed a significant response, and the storm time response was slightly stronger there. In their statistical study, Carter et al. (2015) concluded that geomagnetic storms may or may not follow intense  $dB/dt$  perturbations associated with  $SI^+$  events.

The main goal of this paper is to investigate the effects of IP shock orientations and speeds on the subsequent perturbations of  $dB/dt$  or generation of GICs. This is the largest statistical study of the subject to date and the first to link shock impact angle and speed effects to the subsequent  $dB/dt$  enhancement. We show that  $dB/dt$  is largely intensified by shocks with high speeds that strike Earth nearly head-on. In addition, we show that equatorial GICs may be intensified to extreme levels due to intensifications of the equatorial ionospheric current near local noon caused by shocks with high speeds that first touch the magnetosphere at the subsolar point.

## 2. Currents Associated With Latitudinal GIC Response to $SI^+$ Events

The magnetopause current flows in the magnetopause nose at distances  $> 10$  Earth radii from the ground. During  $SI^+$  events, sudden changes in solar wind dynamic pressure increase the horizontal geomagnetic field component with different latitudinal responses (Russell et al., 1994; Zesta et al., 2000). However, there are two specific ionospheric current systems that are intensified by magnetopause compression which contribute with the generation of GICs. In auroral regions, the auroral electrojet (AEJ) current is intensified by the increase of the Region 1 current (Araki, 1977, 1994). In a narrowly confined latitudinal region of the dayside equatorial ionosphere, the equatorial electrojet (EEJ) current is intensified due to the increase in electric field and conductivity along that region (Lühr et al., 2004; Sibeck, 1991).

GIC enhancements in midlatitude to low-latitude regions are primarily due to magnetopause current enhancements, since the ionospheric electrojets are far away from those regions (Fiori et al., 2014). The magnetopause current effects on GIC production are overshadowed by high-latitude ionospheric currents because the latter are much closer to the ground ( $\sim 100$  km altitude) and therefore produce higher  $dB/dt$  perturbations there (Fiori et al., 2014). AEJ currents are associated with high-latitude GIC enhancements (Boteler et al., 1998; Kappenman, 2005; Pulkkinen et al., 2005), while equatorial GIC enhancements are caused by the EEJ current (Carter et al., 2015, 2016; Ngwira et al., 2013; Pulkkinen et al., 2012). GICs linked to EEJ currents have recently been revealed as an increasing concern to power grids located a few degrees from the magnetic equator (see, e.g., Moldwin & Tsu, 2016). These magnetospheric-ionospheric currents are subject of modeling for cases when the ground geomagnetic field is not available for GIC determinations (de Villiers et al., 2017).

The ultimate goal of this paper is to investigate the effects of IP shock impact angles and speeds on the GIC generation on the ground, which result from the intensification of the currents mentioned above.

## 3. Data Set

### 3.1. IP Shock Database

Our shock database is an extension of the IP shock catalog published by Oliveira and Raeder (2015). This catalog currently contains 547 IP shocks covering a time range over two solar cycles from January 1995 to September 2017. Wind and Advanced Composition Explorer (ACE) solar wind and interplanetary magnetic field (IMF) data were used to compute shock normals and speeds for all events. The shock parameters were calculated by solving the Rankine-Hugoniot conditions, which are based on the conservation of energy and momentum across the shock surface (Burlaga, 1971; Landau & Lifshitz, 1960). The methods and techniques used to compute those and other shock properties are outlined in detail by previous works (Oliveira, 2017; Oliveira & Raeder, 2015; Oliveira & Samsonov, 2018; Oliveira et al., 2016). A list with 547 IP shocks can be found in the supporting information.

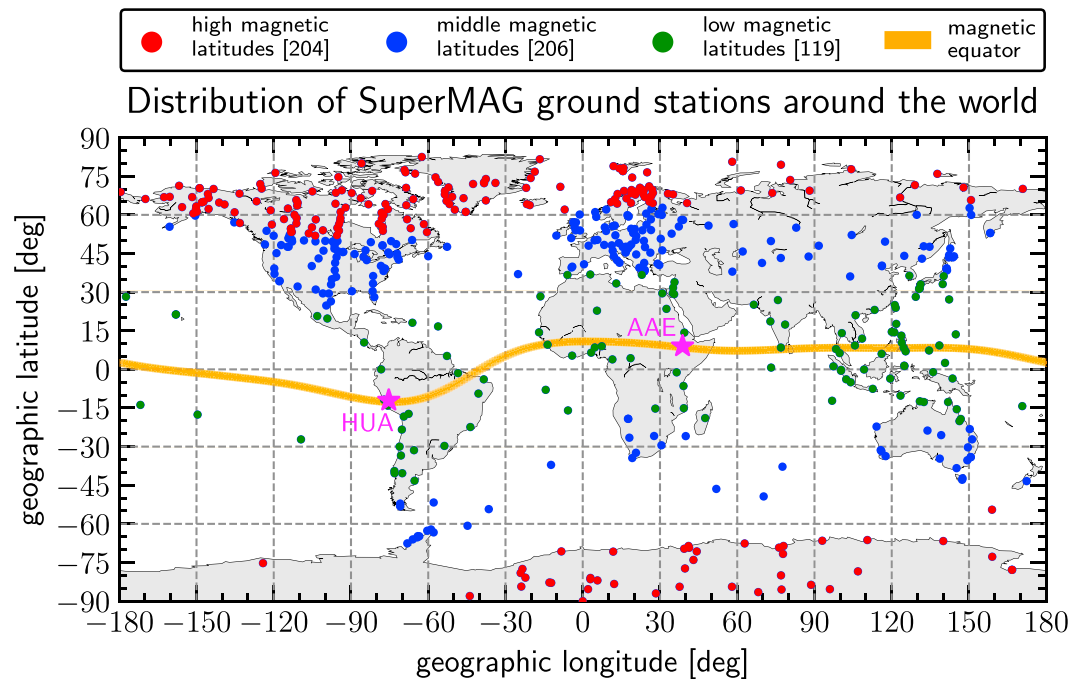


**Figure 1.** Global distribution of ground magnetometer stations that joined the SuperMAG collaboration represented in geographic coordinates. The 528 stations used in this study are divided as follows: 204 high-latitude stations (red dots); 206 midlatitude stations (blue dots), and 119 low-latitude stations (green dots), with colors indicating latitudes in magnetic coordinates. The thick orange curve indicates the geographic position of the magnetic equator. See text for discussion on the Huancayo (HUA) and Addis Ababa (AAE) stations represented by the stars in magenta.

### 3.2. Ground Magnetometer Data

We use global ground magnetometer data from SuperMAG to determine the global  $dB/dt$  response and identify the likely locations for GIC inputs. SuperMAG is a worldwide collaboration with 528 ground magnetometer stations (Gjerloev, 2009, 2012). We also use the SuperMAG partial ring current index, SMR, which is similar to the traditional *SYM-H* index, but more than 100 stations in midlatitude and low-latitude regions are used for its computation (Newell & Gjerloev, 2012). Another important difference between *SYM-H* and SMR is that in the computation of the latter the ring current is not assumed to be constant until late storm recovery phase due to strong local time gradients (Newell & Gjerloev, 2012). The use of such a magnetometer array is recommended because it enhances the quality of regional and global data products as a result of the increasing level of regional and global collaborations (Engebretson & Zesta, 2017).

Figure 1 shows the geographic distribution of the SuperMAG stations used in this study. We divide the stations in three different magnetic latitude (MLAT) regions as follows: high-latitude regions ( $60^\circ < |MLAT| < 90^\circ$ , red dots, 204 stations), midlatitude regions ( $30^\circ < |MLAT| < 60^\circ$ , blue dots, 206 stations), and low-latitude regions ( $-30^\circ < MLAT < 30^\circ$ , green dots, 119 stations). The thick orange curve corresponds to the location of the magnetic equator on the global map.

In this study, GICs are linked to abrupt or step-like changes in the horizontal geomagnetic field,  $dB/dt$ , according to Faraday's law (Pirjola, 2000, 2002; Viljanen, 1998). The total horizontal geomagnetic field is  $B = \sqrt{B_n^2 + B_e^2}$ , with  $B_n$  and  $B_e$  being the measured 1-min time resolution northward and eastward components of the geomagnetic field, respectively. The compression onset is defined by the sudden increase in the SMR index, an  $SI^+$  event signature. In some cases, more than one  $dB/dt$  peak occurs within 1 hr after compression onset, resulting from storm and substorm activity. Since we are primarily interested in the immediate effect caused by magnetospheric and ionospheric current enhancements following IP shock impacts, or the first  $dB/dt$  measured peak, we fixed a time window of 10 min following the shock impact to capture this first peak. In this study, more than 103,000 local ground magnetometer traces were analyzed, with over 12 million data points.

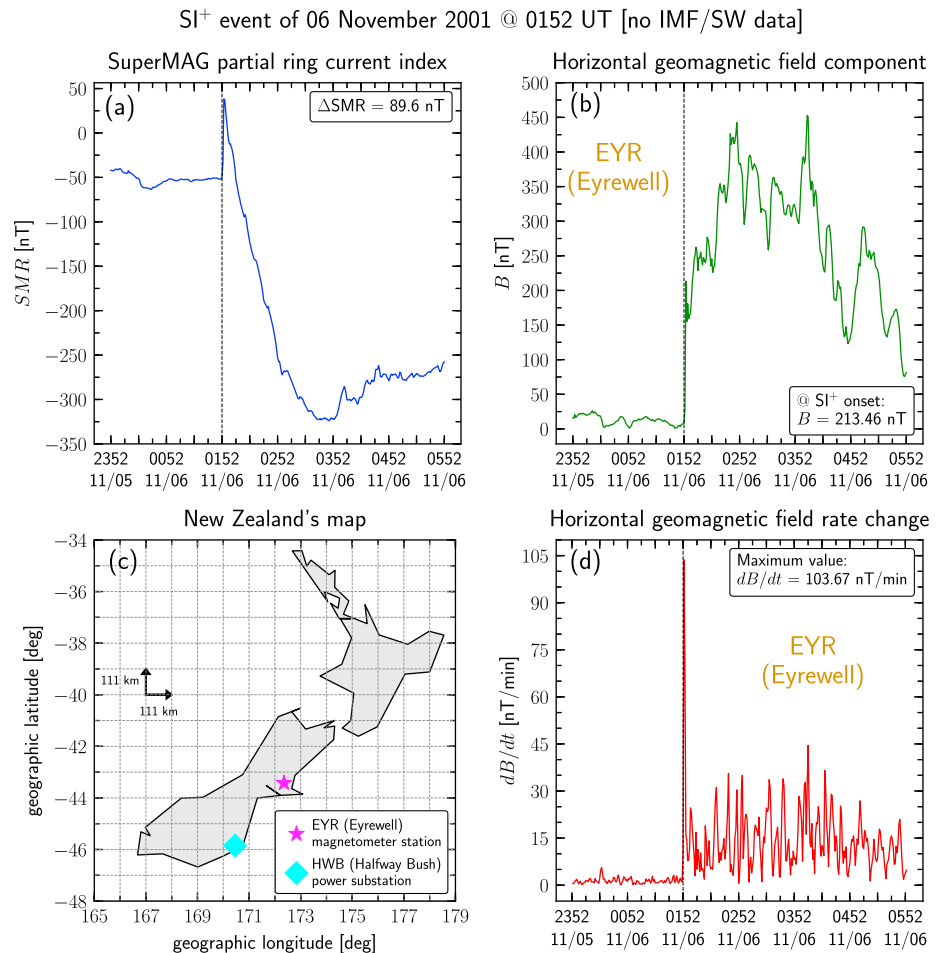


**Figure 2.** Global and local ground magnetometer response to the likely impact of a strong interplanetary shock on the magnetosphere on 6 November 2001. (a) Global SMR index; (b) horizontal geomagnetic field ( $B$ ); (c) New Zealand's map; and (d) change rate of horizontal geomagnetic field ( $dB/dt$ ). The local magnetometer response was recorded by the Eyrewell station (EYR, magenta star on the map). The reported transformer failure occurred in the Halfway Bush power substation (HWB, cyan diamond on the map).

#### 4. Transformer Failure Caused by an SI<sup>+</sup> Event

In this section, we present an SI<sup>+</sup> event that was reported to be the cause of a transformer failure. The geomagnetic storm of 6 November 2001 was an intense space weather event with minimum SMR index of  $-320$  nT. The main phase of that storm was preceded by a strong SI<sup>+</sup> event whose onset occurred at 0152 UT; however, geospace data, that is, solar wind and IMF data upstream of the Earth, are not available on that day for the computations of the driver's properties. This lack of data is most likely due to instrument saturation caused by a strong IP shock driven by a coronal mass ejection (CME).

Figure 2 shows global and local magnetometer response to the potential impact of a CME on the magnetosphere on 6 November 2001. Figure 2a depicts the SMR index, which shows an SI<sup>+</sup> event with amplitude of  $\sim 90$  nT. The minimum SMR measurement occurred  $\sim 2$  hr after SI<sup>+</sup> onset. Local ground magnetometer response is shown in Figure 2b and represented by the horizontal component of geomagnetic field recorded by the midlatitude Eyrewell (EYR, MLAT =  $-50.08^\circ$ ) station located in New Zealand (magenta star on the map, Figure 2c). A strong and sharp field variation coincides with the SI<sup>+</sup> event onset at 0153 UT, with  $dB > 200$  nT within a few minutes. In the subsequent moments,  $B$  continues to vary, but with incremental changes followed by incremental decreases. The change rate of the geomagnetic field recorded by EYR is shown in Figure 2d, whose maximum perturbation corresponds to  $dB/dt \approx 104$  nT/min.

Geomagnetic field perturbations of  $\sim 100$  nT/min as the one recorded by the EYR station are commonly observed by high-latitude stations but are less frequently recorded by stations located in midlatitude

to low-latitude regions (Fiori et al., 2014). The field perturbation shown in Figure 2d is reported by Marshall et al. (2012) to have been the direct cause of the activation of several alarm systems and even a subsequent equipment failure in a power substation in New Zealand. The Halfway Bush (HWB, cyan diamond, Figure 2c) power plant, operated by Transpower New Zealand Ltd, had a transformer completely destroyed by GICs generated by  $dB/dt$  perturbations which were recorded by EYR. The geographic distance between EYR and HWB is about 300 km, and the latitudinal separation, more significant for field variations, is about 220 km. One might argue that this distance is too large. However, Ngwira et al. (2009) were able to model GICs for ground stations separated by almost 600 km. Their consistent results support the assumption that  $dB/dt$  perturbations similar to the one recorded by EYR also took place in HWB. Geomagnetic perturbations of the order of 100 nT/min have been reported to cause some level of power equipment failures in power stations located in regions between  $\pm 60^\circ$  latitudes (Kappenman, 2006). This is a region of growing concern since the number of power plants there has substantially increased in the past decades (Fiori et al., 2014; Gaunt & Coetzee, 2007; Kappenman, 2003, 2006). Fiori et al. (2014) also showed that  $dB/dt$  perturbations  $> 100$  nT/min are observed in midlatitude to low-latitude regions. We then follow Fiori et al.'s (2014) results and take the value 100 nT/min as an indication of a high-risk factor to power plant equipment resulting from the impact of IP shocks on the Earth's magnetosphere.

## 5. Results

### 5.1. Shock Impact Angle and Speed Conventions

In this work, we assume that the shock fronts are planar structures when observed by solar wind monitors at L1, and shock normal vectors are defined in geocentric solar equatorial coordinates pointing in the antisunward direction. Therefore,  $\theta_{x_n} = 180^\circ$  indicates a purely frontal shock. With this convention, the smaller the  $\theta_{x_n}$ , the more inclined the shock. The terminology "small impact angle" implies that the normal vector is almost aligned with the geocentric solar equatorial X line. The shock speed  $v_s$  is measured relative to the Earth or the spacecraft.

### 5.2. Effects of $\theta_{x_n}$ on $SI^+$ RTs and Subsequent $dB/dt$ Perturbations

In order to isolate the effects of shock impact angles on the subsequent  $dB/dt$  intensification, ground magnetometer response to two IP shocks with very similar speeds ( $\sim 560$  km/s) and strengths (magnetosonic Mach numbers  $\sim 2.2$ ), but with very different  $\theta_{x_n}$ , are shown in Figure 3. The left column shows results for the nearly frontal shock ( $\theta_{x_n} = 175.39^\circ$ ) of 11 October 2001 and compression onset at 1658 UT, whereas the right column shows results for the highly inclined shock ( $\theta_{x_n} = 134.96^\circ$ ) of 25 May 2013 and compression onset at 0947 UT. The nearly frontal shock was observed by the equatorial Huancayo (HUA) station, in South America, while the highly inclined shock was observed by the equatorial Addis Ababa (AAE) station, in Africa. Both stations were located at noon local time (LT) at the shock impact time. In Figure 3, the top row shows SMR, in nanotesla, the middle row shows the time derivative of the SMR index, or rate change  $dSMR/dt$ , in nT/min, and the bottom row shows the  $dB/dt$  response, in nT/min.

Figures 3a and 3b show that the effects of shock impact angles are readily seen in the  $SI^+$  signatures as indicated by the SMR index data. The  $SI^+$  event triggered by the nearly frontal shock had an amplitude of  $\sim 50$  nT and RT of 5 min (shaded area in Figure 3a). In contrast, the SMR amplitude associated with the highly inclined shock was smaller ( $\sim 29$  nT), and the RT was significantly larger (16 min, shaded area in Figure 3b), even though both shocks had similar speeds and Mach numbers (strengths). These results are consistent with previous observation and simulation works, which suggested that nearly frontal shocks with high speeds cause  $SI^+$  events with short RTs and large amplitudes (Araki et al., 2004; Guo et al., 2005; Selvakumaran et al., 2017; Takeuchi et al., 2002; Wang et al., 2006). The effects of the shock impact angles are also reflected on the rate of change of the SMR index, where  $dSMR/dt$  is smaller in the case of the highly inclined shock due to its gradual compression of the magnetosphere.

As shown by Figures 3c and 3d, the maximum  $dSMR/dt$  enhancement associated with the nearly frontal shock (21.4 nT/min) is 3 times higher than the one associated with the highly inclined shock (7.2 nT/min). Similarly, Figures 3e and 3f indicate that the maximum  $dB/dt$  measured for the nearly frontal shock is 103.28 nT/min, while the same for the highly inclined shock is 11.81 nT/min. In order to estimate the role of the EEJ current in enhancing  $dB/dt$  perturbations, we compute the maximum amplification ratio  $(dB/dt)/(dSMR/dt)$  for both shocks, as suggested by Carter et al. (2015). This nondimensional factor gives a sense of the fractional magnitude of the geomagnetic perturbation on the ground relative to the magnetopause current perturbation as expressed by the SMR index. In midlatitude or low-latitude regions, this ratio is close to 1. The amplitude ratios

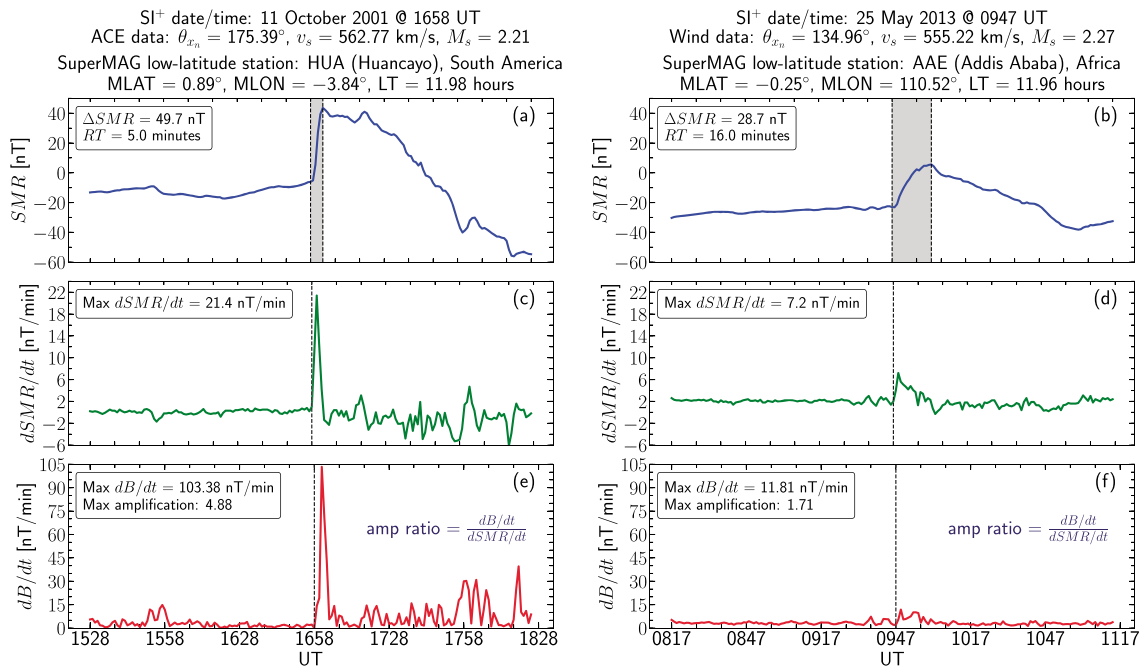


**Figure 3.** Ground magnetometer response to two interplanetary shocks with very similar speeds and magnetosonic Mach numbers (strength) but with very different shock impact angles. (left column) Nearly frontal shock,  $\theta_{x_n} = 175.39^\circ$ ; (right column) highly inclined shock,  $\theta_{x_n} = 134.96^\circ$ . (a and b) SMR index, in nanotesla; (c and d)  $dSMR/dt$ , in nT/min; (e and f)  $dB/dt$ , in nT/min. The shaded areas in (a) and (b) correspond to the  $SI^+$  RTs for both shocks. The amplification factor is defined as the ratio  $(dB/dt)/(dSMR/dt)$ . Huancayo (HUA, South America) indicates response to the nearly frontal shock, while Addis Ababa (AAE, Africa) indicates response to the highly inclined shock. During the shock compression, both stations were right below the EEJ at noon LT (see the magenta stars in Figure 1). SMR = SuperMAG partial ring current index; RT = rise time; EEJ = equatorial electrojet; LT = local time.

obtained are 4.88 and 1.71 recorded by the HUA and AAE stations following the impacts of the nearly frontal and highly inclined shocks, respectively. In fact, the magenta stars of Figure 1 show that the HUA and AAE stations are located very close to the magnetic equator and certainly below the EEJ current system. The amplification is much higher in the nearly frontal shock case because the ground perturbation is very sensitive to sudden magnetospheric compressions often caused by shocks with high speeds that first hit the bow shock at the subsolar point. This indicates that the EEJ current is more intensified by impacts of head-on shocks with high speeds.

Based on the previous findings, one may suggest that the  $SI^+$  event of 6 November 2001 at 0152 UT and the subsequent  $dB/dt$  perturbation associated with the complete destruction of a transformer in the station depicted in Figure 2 was caused by the impact of a very fast and almost head-on shock on the magnetosphere. Despite the fact that there are no ACE and/or Wind data available for that event, the SOHO spacecraft observed a solar wind dynamic pressure enhancement of  $\sim 20$  nPa at 0120 UT at a distance of  $\sim 197$  Earth's radii upstream of the Earth. If the disturbance was a shock, it would have been very fast, with an estimated travel speed of  $\sim 700$  km/s (Marshall et al., 2012). Given the results of this work, we believe the November 2001  $SI^+$  event was most likely caused by the impact of a nearly frontal shock driven by a very fast CME on the Earth's magnetosphere.

### 5.3. Statistical Results

Figure 4 shows shock impact angle  $\theta_{x_n}$ , in degrees, plotted as a function of shock speed  $v_s$ , in km/s. The color bars indicate the strength of the maximum  $dB/dt$  value recorded among all stations located worldwide in each magnetic latitude region, that is, high, middle, and low, with data available for each IP shock. Left-hand side panels indicate results for stations in the dayside, whereas right-hand side panels indicate results for stations in the nightside. In general, as indicated in all panels, nearly frontal shocks tend to have high speed, while highly inclined shocks tend to have low speed. Almost all shocks with low speed, that is,  $v_s < 300$  km/s, have  $\theta_{x_n} < 140^\circ$ , while most high-speed shocks with  $v_s > 600$  km/s are associated with  $\theta_{x_n} > 140^\circ$ . No particular trend is observed for moderate shocks ( $300 \text{ km/s} < v_s < 600 \text{ km/s}$ ). A broader range of  $\theta_{x_n}$  is observed for this category.

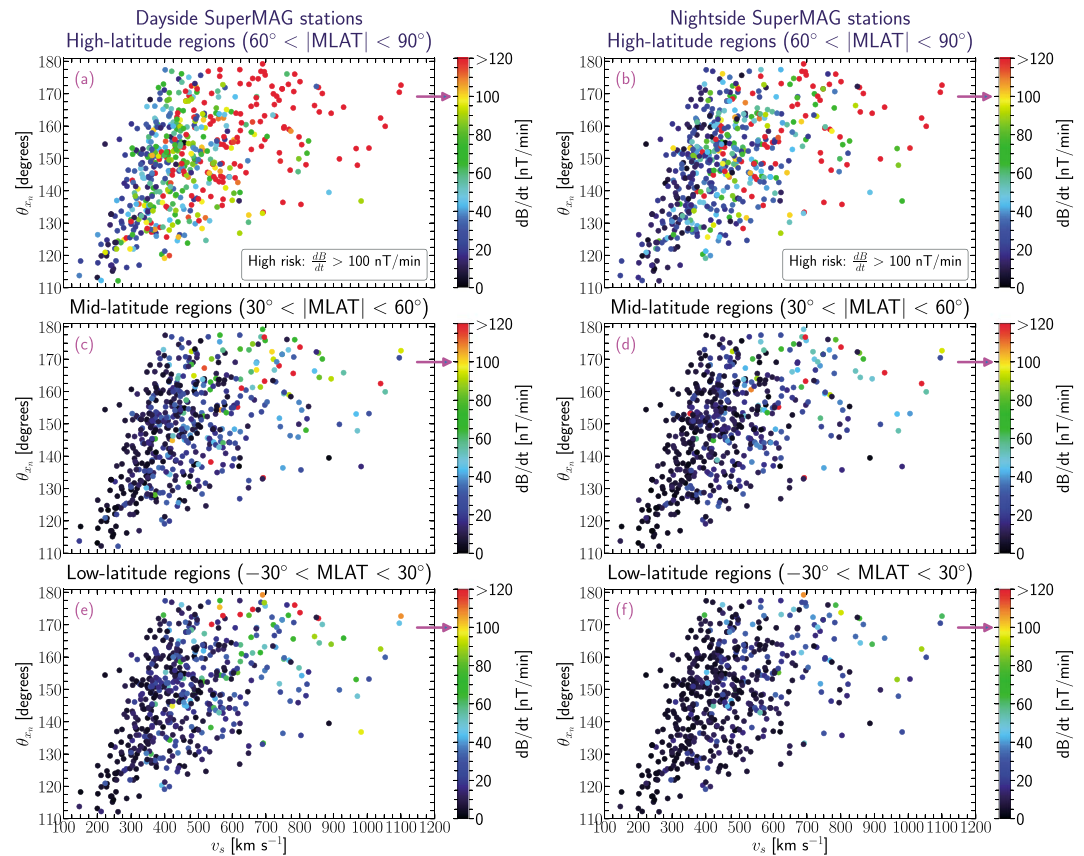


**Figure 4.** Shock impact angle  $\theta_{xn}$  plotted as a function of shock speed  $v_s$ . The color bars indicate the maximum worldwide  $dB/dt$  perturbation value among stations with available data for each shock recorded in a time interval of 10 min after compression onset. The stations are divided in the following regions: dayside (left column); and nightside (right column). (a, b) High latitudes, (c, d) midlatitudes, and (e, f) low latitudes. The arrows in magenta indicate the threshold of 100 nT/min, a high-risk factor posed by GICs to power system components. GICs = geomagnetically induced currents.

Figure 4a shows  $dB/dt$  enhancements for dayside high-latitude stations ( $60^\circ < |MLAT| < 90^\circ$ ). In those regions, most shocks with  $v_s > 400$  km/s and  $\theta_{xn} > 140^\circ$  generate  $dB/dt > 100$  nT/min. In the nightside, as shown by Figure 4b, most perturbations with  $dB/dt > 100$  nT/min are associated with shocks in the same shock speed and impact angle ranges as in those in the dayside. This is explained by the fact that shock impacts cause the first and largest current system perturbations in the dayside, intensifying both hemispheres' AEJ currents (Boudouridis et al., 2005; Shi et al., 2017; Zesta et al., 2000); the nightside will respond later due to field-aligned currents connected to the tail which may trigger, for example, substorms (Akasofu, 1964; McPherron, 1991; Oliveira & Raeder, 2014, 2015). Much weaker responses are observed in midlatitude regions (Figures 4c and 4d) compared to high-latitude responses.

Enhancements in  $dB/dt$  in the dayside low-latitude regions are shown by Figure 4e. Most shocks with  $v_s < 500$  km/s are associated with  $dB/dt < 30$  nT/min, but a few events triggered  $dB/dt$  around 60 nT/min. In the cases with  $v_s > 500$  km/s,  $dB/dt$  enhancements were usually larger than 30 nT/min, with some events with  $dB/dt$  around 80 nT/min. However, there are nine events with  $dB/dt$  perturbations surpassing the high-risk threshold of 100 nT/min. The characteristics and uniqueness of these events will be discussed below.

Maximum enhancements in  $dB/dt$  were recorded for the nine events by the equatorial HUA, AAE, and Davao (A08, Southeast Asia) stations. The corresponding magnetic latitudes of these stations, along with the shock properties and subsequent geomagnetic field responses, are shown in Table 1. All shocks associated with high-risk levels of  $dB/dt$  have impact angles near  $180^\circ$  and shock speeds associated with moderate to strong shocks, or  $v_s > 550$  km/s. In all cases, the shocks were precursors of some level of geomagnetic activity, with minimum SMR indices indicating values below  $-71$  nT. The 7 November 2004 IP shock caused the largest

**Table 1**

General Aspects of IP Shock Parameters and Ground Magnetometer Response of the Events With High-risk Geomagnetic Perturbation ( $dB/dt > 100$  nT/min) Shown in Figure 4e

SI <sup>+</sup> event date/UT	Ground magnetometer response at equatorial stations with high-risk $dB/dt$ perturbations								
	Impact angle $\theta_{x_n}$ (deg)	Shock speed $v_s$ (km/s)	Ground station code	Station LT (hr)	Maximum $dB/dt$ (nT/min)	Maximum $dSMR/dt$ (nT/min)	Maximum amplification ratio	Storm following SI <sup>+</sup> ?	Minimum SMR (nT)
11 Oct 2001/1658	175.39	562.77	HUA <sup>a</sup>	11.98	103.38	16.85	6.14	Yes	-89
21 Oct 2001/1647	173.13	623.69	HUA	11.76	175.87	25.35	6.94	Yes	-219
17 Apr 2002/1106	170.08	538.86	AAE <sup>b</sup>	13.68	133.79	20.65	6.48	Yes	-151
24 Oct 2003/1523	174.71	660.47	HUA	10.36	166.09	25.00	6.64	Yes	-71
7 Nov 2004/1827	176.03	649.06	HUA	13.43	207.64	31.25	6.64	Yes	-394
9 Nov 2004/0928	171.93	855.60	HUA	13.78	172.07	32.07	5.26	Yes	-282
21 Jan 2005/1711	172.63	1099.99	HUA	12.16	109.57	31.05	3.53	Yes	-101
17 Mar 2015/0445	172.79	572.19	A08 <sup>c</sup>	13.15	186.26	26.50	7.03	Yes	-233
22 Jun 2015/1833	173.73	800.81	HUA	13.53	119.47	46.15	2.59	Yes	-204

Note. The UTs indicated in the table correspond to the shock/magnetosphere interaction onset, that is, the instance of time when the SMR index begins to increase in response to the magnetospheric compression.

<sup>a</sup>Huancayo (HUA) station, MLAT = 0.89°, South American sector. <sup>b</sup>Addis Ababa (AAE) station, MLAT = -0.25°, African sector. <sup>c</sup>Davao (A08) station, MLAT = -1.16°, Southeastern Asia sector. A08 is not an IAGA code. This station is operated by the AMBER magnetometer array.

$dB/dt$  enhancement (207.64 nT/min) and was followed by one of the most severe geomagnetic storms in recent history with minimum SMR = -394 nT. However, the largest observed equatorial vertical drifts are associated with the storm on 9 November 2004 (Fejer et al., 2007). Another common aspect of the equatorial  $dB/dt$  response corresponds to the stations' LTs at the shock impact times. In all cases, the stations were located around noon LT; the farthest station was located less than 2 hr of LT away from noon. All events show significant amplification ratio values (>6 for six events), which indicate a high contribution of EEJ currents to  $dB/dt$  enhancements. This agrees with the results of Carter et al. (2015), who showed that EEJ currents intensify  $dB/dt$  response to shocks at equatorial regions. Our results show that nearly frontal and high-speed shocks are an important factor in the generation of high-risk  $dB/dt$  perturbations in equatorial regions. The combination of the LT of the stations at the compression onsets and these shock parameters greatly contribute to the production of high-level  $dB/dt$  perturbations.

Carter et al. (2016) reported that the 2015 St. Patrick's Day geomagnetic storm caused elevated rates of GICs in high-latitude regions during localized storm time substorms, while large GIC enhancements were observed by equatorial stations right after the SI<sup>+</sup> event caused by the precursor shock impact (see also Zhang et al., 2015). The authors attributed high-latitude GIC enhancements to AEJ current intensifications and equatorial GIC enhancements observed by stations at noon LT to EEJ current intensifications. Carter et al. (2015) found large  $dB/dt$  perturbations in equatorial stations following impacts of IP shocks preceding geomagnetic storms, which was later confirmed by Carter et al. (2016). Our results confirm these observations, since all shocks with equatorial responses of  $dB/dt > 100$  nT/min were followed by geomagnetic storms with significant intensity, that is, SMR < -100 nT (see Table 1). This present work confirms those results, with the additional contribution concerning the intensification effects caused by high-speed, nearly frontal shock impacts due to strong and symmetric dayside magnetospheric compression combined with the station location around noon LT during shock impact.

## 6. Conclusions

Effects of IP shock impact angles and speeds on the local variability of geomagnetic field perturbations detected by ground stations were investigated for the first time in this paper. A catalog of 547 IP shocks and a worldwide magnetometer chain with 528 ground stations were used in this study. Subtle changes in the horizontal geomagnetic field component,  $dB/dt$ , an important quantity for producing GICs, were analyzed. For each shock, the maximum  $dB/dt$  perturbation recorded by worldwide stations located in three different latitude regions was investigated as a function of its shock impact angle and speed. The main results of this work are summarized below:

1. In general, low-speed shocks are also highly inclined shocks, while high-speed shocks are nearly frontal shocks. Moderate shocks, that is, shocks with speeds around 500 km/s, are associated with a broader range of shock impact angles, but they tend to be slightly more frontal. These results confirm previous findings that indicate that shocks with high speeds have small impact angles (e.g., Kilpua et al., 2015; Oliveira & Raeder, 2015).
2. We found that in general, large  $dB/dt$  perturbations are associated with high-speed and nearly frontal shocks. The impact of shocks with these properties are known to cause  $SI^+$  events with large amplitudes and short RTs (Araki et al., 2004; Guo et al., 2005; Selvakumaran et al., 2017; Takeuchi et al., 2002; Wang et al., 2006). These effects are explained by the sudden and effective magnetospheric compression leading to high intensification of the ionospheric-magnetospheric current system and subsequent intense geomagnetic activity (Oliveira & Raeder, 2014, 2015; Samsonov et al., 2015).
3. Maximum values of  $dB/dt$  perturbations are shown to depend significantly on shock impact angles and speeds in all magnetic latitude regions. In the dayside high-latitude regions, most shocks with  $v_s > 400$  km/s and  $\theta_{x_n} > 140^\circ$  surpass the threshold of  $dB/dt = 100$  nT/min, a risk factor that may increase GIC risk (Béland & Small, 2005; Fiori et al., 2014; Kappenman, 2003, 2006; Marshall et al., 2012). The same trend was observed for the nightside high-latitude response, but fewer events showed  $dB/dt > 100$  nT/min. Midlatitude and low-latitude responses were much weaker, with the dayside perturbations being slightly larger than the nightside perturbations.
4. We found nine events in the low-latitude category with  $dB/dt > 100$  nT/min (see Table 1). All these events were caused by high-speed and nearly frontal shocks and were observed by equatorial stations located right below the EEJ current system around noon LT at the time of shock impact. Such high-risk values were observed because the ground perturbation was highly amplified by the EEJ current system (Carter et al., 2015). We report for the first time that very fast shocks with small impact angles increase EEJ current system effects due to a sudden and strong compression of the magnetosphere with direct implications to GIC production rates in the dayside equatorial region.

#### Acknowledgments

D. M. O. acknowledges the NASA-SR grants 13-SRITM13\_2-0011 and HSR-MAG14\_2-0062 under contract with UMBC. B. A. C. was supported by the Australian Research Council Linkage grant LP160100561.

C. M. N. was supported via NASA grant NNG11PL10A 670.157 to CUA/IACS. The 1-min time resolution SuperMAG data are readily available at the SuperMAG website <http://supermag.jhuapl.edu/>. For the ground magnetometer data we gratefully acknowledge Intermagnet; USGS, Jeffrey J. Love; CARISMA, Pi Ian Mann; CANMOS; the S-RAMP Database, Pi K. Yumoto and K. Shiokawa; the SPIDR database; AARI, Pi Oleg Troshichev; the MACCS program, Pi M. Engebretson, Geomagnetism Unit of the Geological Survey of Canada; GIMA; MEASURE, UCLA IGPP and Florida Institute of Technology; SAMBA, Pi Eftyhia Zesta; AMBER, Pi Endawoke Yizengaw; 210 Chain, Pi K. Yumoto; SAMNET, Pi Farideh Honary; the institutes that maintain the IMAGE magnetometer array, Pi Eija Tanskanen; PENGUIN; AUTUMN, Pi Martin Connors; DTU Space, Pi Rico Behlke; South Pole and McMurdo Magnetometer, PIs Louis J. Lanzarotti and Alan T. Weatherwax; ICESTAR; RAPIDMAG; PENGUIN; British Antarctic Survey; McMac, Pi Peter Chi; BGS, Pi Susan Macmillan; Pushkov Institute of Terrestrial Magnetism, Ionosphere and Radio Wave Propagation (IZMIRAN); GFZ, Pi Juergen Matzka; MFGI, Pi B. Heilig; IGFPAS, Pi J. Reda; University of L'Aquila, Pi M. Vellante; BCMT, V. Lesur and A. Chambodut; data obtained in cooperation with Geoscience Australia, Pi Marina Costelloe; and SuperMAG, Pi Jesper W. Gjerloev.

Furthermore, the findings of this work may provide insights for direct applications to space weather forecasting. Solar wind monitors at the L1 point such as Wind and ACE offer real-time solar wind and IMF conditions that are used for automated computations of shock impact angles and speeds (Kruparova et al., 2013; Paulson et al., 2012; Vortnikov et al., 2008, 2011). Therefore, a 30–60 min window time may provide the opportunity to power plant operators to take actions to prevent GICs that may be triggered by high-speed and head-on shocks that will impact the magnetosphere when the station is located around noon LT.

#### References

- Akasofu, S.-I. (1964). The development of the auroral substorm. *Planetary and Space Science*, *12*(4), 273–282. [https://doi.org/10.1016/0032-0633\(64\)90151-5](https://doi.org/10.1016/0032-0633(64)90151-5)
- Albertson, V. D., Bozoki, B., Feero, W. E., Kappenman, J. G., Larsen, E. V., Nordell, D., et al. (1993). Geomagnetic disturbance effects on power systems. *IEEE Transactions on Power Delivery*, *8*(3), 1206–1216. <https://doi.org/10.1109/61.252646>
- Araki, T. (1977). Global structure of geomagnetic sudden commencements. *Planetary and Space Science*, *25*(4), 373–384. [https://doi.org/10.1016/0032-0633\(77\)90053-8](https://doi.org/10.1016/0032-0633(77)90053-8)
- Araki, T. (1994). A physical model of the geomagnetic sudden commencement. In M. J. Engebretson, K. Takahashi, & M. Scholer (Eds.), *Solar wind sources of magnetospheric ultra-low-frequency waves Geophysical Monograph Series* (Vol. 81, pp. 183–200). Washington, DC: American Geophysical Union. <https://doi.org/10.1029/GM081p0183>
- Araki, T., Takeuchi, T., & Araki, Y. (2004). Rise time of geomagnetic sudden commencements—Statistical analysis of ground geomagnetic data. *Earth, Planets and Space*, *56*(2), 289–293. <https://doi.org/10.1186/BF03353411>
- Barbosa, C. S., Caraballo, R., Alves, L. R., Hartmann, G. A., Beggan, C. D., Viljanen, A., et al. (2017). The Tsallis statistical distribution applied to geomagnetically induced currents. *Space Weather*, *15*, 1094–1101. <https://doi.org/10.1002/2017SW001631>
- Barbosa, C. S., Hartmann, G. A., & Pinheiro, K. J. (2015). Numerical modeling of geomagnetically induced currents in a Brazilian transmission line. *Advances in Space Research*, *55*(4), 1168–1179. <https://doi.org/10.1016/j.asr.2014.11.008>
- Béland, J., & Small, K. (2005). Space weather effects on power transmission systems: The cases of Hydro-Québec and Transpower New Zealand Ltd. In I. A. Daglis (Ed.), *Effects of space weather on technology infrastructure* (pp. 287–299). Dordrecht, Netherlands: Springer. <https://doi.org/10.1007/1-4020-2754-015>
- Blake, S. P., Gallagher, P. T., McCauley, J., Jones, A. G., Hogg, C., Campy, J., et al. (2016). Geomagnetically induced currents in the Irish power network during geomagnetic storms. *Space Weather*, *14*, 1136–1154. <https://doi.org/10.1002/2016SW001534>
- Bolduc, L. (2002). GIC observations and studies in the Hydro-Québec power system. *Journal of Atmospheric and Solar-Terrestrial Physics*, *64*(16), 1793–1802. [https://doi.org/10.1016/S1364-6826\(02\)00128-1](https://doi.org/10.1016/S1364-6826(02)00128-1)
- Boteler, D. H., & Pirjola, R. J. (2017). Modeling geomagnetically induced currents. *Space Weather*, *15*, 258–276. <https://doi.org/10.1002/2016SW001499>
- Boteler, D. H., Pirjola, R. J., & Nevanlinna, H. (1998). The effects of geomagnetic disturbances on electrical systems at the Earth's surface. *Advances in Space Research*, *22*(1), 17–27. [https://doi.org/10.1016/S0273-1177\(97\)01096-X](https://doi.org/10.1016/S0273-1177(97)01096-X)

- Boudouridis, A., Zesta, E., Lyons, L. R., Anderson, P. C., & Lummerzheim, D. (2005). Enhanced solar wind geoeffectiveness after a sudden increase in dynamic pressure during southward IMF orientation. *Journal of Geophysical Research*, *110*, A05214. <https://doi.org/10.1029/2004JA010704>
- Burlaga, L. F. (1971). Hydromagnetic waves and discontinuities in the solar wind. *Space Science Reviews*, *12*(5), 600–657. <https://doi.org/10.1007/BF00173345>
- Carter, B. A., Yizengaw, E., Pradipta, R., Halford, A. J., Norman, R., & Zhang, K. (2015). Interplanetary shocks and the resulting geomagnetically induced currents at the equator. *Geophysical Research Letters*, *42*, 6554–6559. <https://doi.org/10.1002/2015GL065060>
- Carter, B. A., Yizengaw, E., Pradipta, R., Weygand, J. M., Piersanti, M., Pulkkinen, A., et al. (2016). Geomagnetically induced currents around the world during the March 17, 2015 storm. *Journal of Geophysical Research: Space Physics*, *121*, 10,496–10,507. <https://doi.org/10.1002/2016JA023344>
- Cassak, P. A., Emslie, A. G., Halford, A. J., Baker, D. N., Spence, H. E., Avery, S. K., & Fisk, L. A. (2017). Space physics and policy for contemporary society. *Journal of Geophysical Research: Space Physics*, *122*, 4430–4435. <https://doi.org/10.1002/2017JA024219>
- de Villiers, J. S., Kosch, M., Yamazaki, Y., & Lotz, S. (2017). Influences of various magnetospheric and ionospheric current systems on geomagnetically induced currents around the world. *Space Weather*, *15*, 403–417. <https://doi.org/10.1002/2016SW001566>
- Eastwood, J. P., Biffis, E., Hapgood, M. A., Green, L., Bisi, M. M., Bentley, R. D., et al. (2017). The economic impact of space weather: Where do we stand? *Risk Analysis*, *37*(2), 206–218. <https://doi.org/10.1111/risa.12765>
- Engbretonson, M., & Zesta, E. (2017). The future of ground magnetometer arrays in support of space weather monitoring and research. *Space Weather*, *15*, 1433–1441. <https://doi.org/10.1002/2017SW001718>
- Fejer, B. G., Jensen, J. W., Kikuchi, T., Abdu, M. A., & Chau, J. L. (2007). Equatorial ionospheric electric fields during the November 2004 magnetic storm. *Journal of Geophysical Research*, *112*, A10304. <https://doi.org/10.1029/2007JA012376>
- Fiori, R. A. D., Boteler, D. H., & Gillies, D. M. (2014). Assessment of GIC risk due to geomagnetic sudden commencements and identification of the current systems responsible. *Space Weather*, *12*, 76–91. <https://doi.org/10.1002/2013SW000967>
- Forbes, K. F., & St. Cyr, O. C. (2008). Solar activity and economic fundamentals: Evidence from 12 geographically disparate power grids. *Space Weather*, *6*, S10003. <https://doi.org/10.1029/2007SW000350>
- Gaunt, C. T. (2016). Why space weather is relevant to electrical power systems. *Space Weather*, *14*, 2–9. <https://doi.org/10.1002/2015SW001306>
- Gaunt, C., & Coetzee, G. (2007). Transformer failures in regions incorrectly considered to have low GIC-risk. In *Power Tech, 2007 IEEE Lausanne* (pp. 807–812). Lausanne, Switzerland: IEEE. <https://doi.org/10.1109/PCT.2007.4538419>
- Gjerloev, J. W. (2009). A global ground-based magnetometer initiative. *Eos, Transactions American Geophysical Union*, *90*(27), 230–231. <https://doi.org/10.1029/2009EO270002>
- Gjerloev, J. W. (2012). The SuperMAG data processing technique. *Journal of Geophysical Research*, *117*, A09213. <https://doi.org/10.1029/2012JA017683>
- Gonzalez, W. D., Joselyn, J. A., Kamide, Y., Kroehl, H. W., Rostoker, G., Tsurutani, B. T., & Vasyliūnas, V. M. (1994). What is a geomagnetic storm? *Journal of Geophysical Research*, *99*(A4), 5771–5792. <https://doi.org/10.1029/93JA02867>
- Guo, X.-C., Hu, Y.-Q., & Wang, C. (2005). Earth's magnetosphere impinged by interplanetary shocks of different orientations. *Chinese Physics Letters*, *22*(12), 3221–3224. <https://doi.org/10.1088/0256-307X/22/12/067>
- Jonas, S., & McCarron, E. (2015). Recent U.S. policy developments addressing the effects of geomagnetically induced currents. *Space Weather*, *13*, 730–733. <https://doi.org/10.1002/2015SW001310>
- Kappenman, J. G. (2003). Storm sudden commencement events and the associated geomagnetically induced current risks to ground-based systems at low-latitude and midlatitude locations. *Space Weather*, *1*(3), 1016. <https://doi.org/10.1029/2003SW000009>
- Kappenman, J. G. (2005). An overview of the impulsive geomagnetic field disturbances and power grid impacts associated with the violent Sun-Earth connection events of 29–31 October 2003 and a comparative evaluation with other contemporary storms. *Space Weather*, *3*, 08C01. <https://doi.org/10.1029/2004SW000128>
- Kappenman, J. G. (2006). Great geomagnetic storms and extreme impulsive geomagnetic field disturbance events—An analysis of observational evidence including the great storm of May 1921. *Advances in Space Research*, *38*(2), 188–199. <https://doi.org/10.1016/j.asr.2005.08.055>
- Kilpua, E. K. J., Lumme, K., Andréová, E., Isavnin, A., & Koskinen, H. E. J. (2015). Properties and drivers of fast interplanetary shocks near the orbit of the Earth (1995–2013). *Journal of Geophysical Research: Space Physics*, *120*, 4112–4125. <https://doi.org/10.1002/2015JA021138>
- Knipp, D. J. (2015). Forward to space weather collection on geomagnetically induced currents: Commentary and research. *Space Weather*, *13*, 742–746. <https://doi.org/10.1002/2015SW001318>
- Kruparova, O., Maksimovic, M., Šafránková, J., Nemeček, Z., Santolik, O., & Krupar, V. (2013). Automated interplanetary shock detection and its application to Wind observations. *Journal of Geophysical Research*, *118*, 4793–4803. <https://doi.org/10.1002/jgra.50468>
- Landau, L. D., & Lifshitz, E. M. (1960). *Electrodynamics of continuous media*. Oxford, England: Pergamon Press.
- Lühr, H., Maus, S., & Rother, M. (2004). Noon-time equatorial electrojet: Its spatial features as determined by the CHAMP satellite. *Journal of Geophysical Research*, *109*, A01306. <https://doi.org/10.1029/2002JA009656>
- Marshall, R. A., Dalzell, M., Waters, C. L., Goldthorpe, P., & Smith, E. A. (2012). Geomagnetically induced currents in the New Zealand power network. *Space Weather*, *10*, S08003. <https://doi.org/10.1029/2012SW000806>
- McPherron, M. L. (1991). Physical processes producing magnetospheric substorms and magnetic storms. In *Geomagnetism* (Vol. 4, pp. 7). Cambridge, MA: Academic Press Ltd.
- Moldwin, M. B., & Tsu, J. S. (2016). Stormtime equatorial electrojet ground-induced currents. In T. Fuller-Rowell, E. Yizengaw, P. H. Doherty, & S. Basu (Eds.), *Ionospheric Space Weather, Geophysical Monograph Series* (Vol. 220, pp. 33–40). Washington, DC: American Geophysical Union. <https://doi.org/10.1002/9781118929216.ch3>
- National Research Council (2008). Severe space weather events—Understanding societal and economic impacts: A workshop report (Tech. Rep.). Washington, DC: National Research Council (NRC).
- Newell, P. T., & Gjerloev, J. W. (2012). SuperMAG-based partial ring current indices. *Journal of Geophysical Research*, *117*, A05215. <https://doi.org/10.1029/2012JA017586>
- Ngwira, C. M., McKinnell, L.-A., Cilliers, P. J., Viljanen, A., & Pirjola, R. (2009). Limitations of the modeling of geomagnetically induced currents in the South African power network. *Space Weather*, *7*, 10002. <https://doi.org/10.1029/2009SW000478>
- Ngwira, C. M., Pulkkinen, A., Wilder, F. D., & Crowley, G. (2013). Extended study of extreme geoelectric field event scenarios for geomagnetically induced current applications. *Space Weather*, *11*, 121–131. <https://doi.org/10.1002/swe.20021>
- Oliveira, D. M. (2017). Magnetohydrodynamic shocks in the interplanetary space: A theoretical review. *Brazilian Journal of Physics*, *47*(1), 81–95. <https://doi.org/10.1007/s13538-016-0472-x>

- Oliveira, D. M., & Ngwira, C. M. (2017). Geomagnetically induced currents: Principles. *Brazilian Journal of Physics*, 47(5), 552–560. <https://doi.org/10.1007/s13538-017-0523-y>
- Oliveira, D. M., & Raeder, J. (2014). Impact angle control of interplanetary shock geoeffectiveness. *Journal of Geophysical Research: Space Physics*, 119, 8188–8201. <https://doi.org/10.1002/2014JA020275>
- Oliveira, D. M., & Raeder, J. (2015). Impact angle control of interplanetary shock geoeffectiveness: A statistical study. *Journal of Geophysical Research: Space Physics*, 120, 4313–4323. <https://doi.org/10.1002/2015JA021147>
- Oliveira, D. M., Raeder, J., Tsurutani, B. T., & Gjerloev, J. W. (2016). Effects of interplanetary shock inclinations on nightside auroral power intensity. *Brazilian Journal of Physics*, 46(1), 97–104. <https://doi.org/10.1007/s13538-015-0389-9>
- Oliveira, D. M., & Samsonov, A. A. (2018). Geoeffectiveness of interplanetary shocks controlled by impact angles: A review. *Advances in Space Research*, 61(1), 1–44. <https://doi.org/10.1016/j.asr.2017.10.006>
- Oughton, E. J., Skelton, A., Horne, R. B., Thomson, A. W. P., & Gaunt, C. T. (2017). Quantifying the daily economic impact of extreme space weather due to failure in electricity transmission infrastructure. *Space Weather*, 15, 65–83. <https://doi.org/10.1002/2016SW001491>
- Paulson, K. W., Taylor, D. K., Smith, C. W., Vasquez, B. J., & Hu, Q. (2012). Advance warning of high-speed ejecta based on real-time shock analyses: When fast-moving ejecta appear to be overtaking slow-moving shocks. *Space Weather*, 10, S12002. <https://doi.org/10.1029/2012SW000855>
- Piccinelli, R., & Krausmann, E. (2018). North Europe power transmission system vulnerability during extreme space weather. *Journal of Space Weather and Space Climate*, 8(A03), 12. <https://doi.org/10.1051/swsc/2017033>
- Pirjola, R. (2000). Geomagnetically induced currents during magnetic storms. *IEEE Transactions on Plasma Science*, 28(6), 1867–1873. <https://doi.org/10.1109/27.902215>
- Pirjola, R. (2002). Review on the calculation of surface electric and magnetic fields and of geomagnetically induced currents in ground-based technological systems. *Surveys in Geophysics*, 23(1), 71–90. <https://doi.org/10.1023/A:1014816009303>
- Pulkkinen, A. (2015). Geomagnetically induced currents modeling and forecasting. *Space Weather*, 13, 734–736. <https://doi.org/10.1002/2015SW001316>
- Pulkkinen, A., Bernabeu, E., Eichner, J., Beggan, C., & Thomson, A. W. P. (2012). Generation of 100-year geomagnetically induced current scenarios. *Space Weather*, 10, S04003. <https://doi.org/10.1029/2011SW000750>
- Pulkkinen, A., Bernabeu, E., Thomson, A., Viljanen, A., Pirjola, R., Boteler, D., et al. (2017). Geomagnetically induced currents: Science, engineering, and applications readiness. *Space Weather*, 15, 828–856. <https://doi.org/10.1002/2016SW001501>
- Pulkkinen, A., Lindahl, S., Viljanen, A., & Pirjola, R. (2005). Geomagnetic storm of 29–31 October 2003: Geomagnetically induced currents and their relation to problems in the Swedish high-voltage power transmission system. *Space Weather*, 3, 1. <https://doi.org/10.1029/2004SW000123>
- Russell, C. T., Ginsky, M., & Petrinec, S. M. (1994). Sudden impulses at low-latitude stations: Steady state response for northward interplanetary magnetic field. *Journal of Geophysical Research*, 99(A1), 253–261. <https://doi.org/10.1029/93JA02288>
- Samsonov, A. A., Sergeev, V. A., Kuznetsova, M. M., & Sibeck, D. G. (2015). Asymmetric magnetospheric compressions and expansions in response to impact of inclined interplanetary shock. *Geophysical Research Letters*, 42, 4716–4722. <https://doi.org/10.1002/2015GL064294>
- Schrijver, C. J., Dobbins, R., Murtagh, W., & Petrinec, S. M. (2014). Assessing the impact of space weather on the electric power grid based on insurance claims for industrial electrical equipment. *Space Weather*, 12, 487–498. <https://doi.org/10.1002/2014SW001066>
- Schulte in den Bäumen, H., Moran, D., Lenzen, M., Cairns, I., & Steenge, A. (2014). How severe space weather can disrupt global supply chains. *Natural Hazards and Earth System Sciences*, 14(10), 2749–2759. <https://doi.org/10.5194/nhess-14-2749-2014>
- Selvakumaran, R., Veenadhari, B., Ebihara, Y., Kumar, S., & Prasad, D. S. V. D. (2017). The role of interplanetary shock orientation on SC/SI rise time and geoeffectiveness. *Advances in Space Research*, 59(5), 1425–1434. <https://doi.org/10.1016/j.asr.2016.12.010>
- Shi, Y., Zesta, E., Connor, H. K., Su, Y.-J., Sutton, E. K., Huang, C. Y., et al. (2017). High-latitude thermosphere neutral density response to solar wind dynamic pressure enhancement. *Journal of Geophysical Research: Space Physics*, 122, 11,559–11,578. <https://doi.org/10.1002/2017JA023889>
- Sibeck, D. G. (1991). The magnetospheric and ionospheric response to solar wind dynamic pressure variations. In *Modeling magnetospheric plasma processes, Geophysical Monograph Series* (Vol. 62, pp. 1–8). Washington, DC: American Geophysical Union. <https://doi.org/10.1029/GM062p0001>
- Smith, E. J., Slavin, J. A., Zwickl, R. D., & Bame, S. J. (1986). Shocks and storm sudden commencements. In Y. Kamide & J. A. Slavin (Eds.), *Solar wind and magnetosphere coupling* (pp. 345). Tokyo, Japan: Terra Scientific.
- Takeuchi, T., Russell, C. T., & Araki, T. (2002). Effect of the orientation of interplanetary shock on the geomagnetic sudden commencement. *Journal of Geophysical Research*, 107(A12), 1423. <https://doi.org/10.1029/2002JA009597>
- Torta, J. M., Marcuello, A., Campanyà, J., Marsal, S., Queral, P., & Ledo, J. (2017). Improving the modeling of geomagnetically induced currents in Spain. *Space Weather*, 15, 691–703. <https://doi.org/10.1002/2017SW001628>
- Tsurutani, B. T., & Lin, R. P. (1985). Acceleration of >47 keV ions and >2 keV electrons by interplanetary shocks at 1 AU. *Journal of Geophysical Research*, 90(A1), 1–11. <https://doi.org/10.1029/JA090iA01p00001>
- Viljanen, A. (1998). Relation of geomagnetically induced currents and local geomagnetic variations. *IEEE Transactions on Power Delivery*, 13(4), 1285–1290. <https://doi.org/10.1109/61.714497>
- Vorotnikov, V. S., Smith, C. W., Farrugia, C. J., Meredith, C. J., Hu, Q., Szabo, A., et al. (2011). Use of single-component wind speed in Rankine-Hugoniot analysis of interplanetary shocks. *Space Weather*, 9, S04001. <https://doi.org/10.1029/2010SW000631>
- Vorotnikov, V. S., Smith, C. W., Hu, Q., Szabo, A., Skoug, R. M., & Cohen, C. M. S. (2008). Automated shock detection and analysis algorithm for space weather application. *Space Weather*, 6, S03002. <https://doi.org/10.1029/2007SW000358>
- Wang, C., Li, C. X., Huang, Z. H., & Richardson, J. D. (2006). Effect of interplanetary shock strengths and orientations on storm sudden commencement rise times. *Geophysical Research Letters*, 33, L14104. <https://doi.org/10.1029/2006GL025966>
- Wik, M., Viljanen, A., Pirjola, R., Pulkkinen, A., Wintoft, P., & Lundstedt, H. (2008). Calculation of geomagnetically induced currents in the 400 kV power grid in southern Sweden. *Space Weather*, 6, S07005. <https://doi.org/10.1029/2007SW000343>
- Zesta, E., Singer, H. J., Lummerzheim, D., Russell, C. T., Lyons, L. R., & Brittner, M. J. (2000). The effect of the January 10, 1997, pressure pulse on the magnetosphere-ionosphere current system. In S. -I. Ohtani, R. Fujii, M. Hesse, & R. L. Lysak (Eds.), *Magnetospheric current systems, Geophysical Monograph Series* (Vol. 118, pp. 217–226). Washington, DC: American Geophysical Union. <https://doi.org/10.1029/GM118p0217>
- Zhang, J. J., Wang, C., Sun, T. R., & Liu, Y. D. (2016). Risk assessment of the extreme interplanetary shock of 23 July 2012 on low-latitude power networks. *Space Weather*, 14, 259–270. <https://doi.org/10.1002/2015SW001347>
- Zhang, J. J., Wang, C., Sun, T. R., Liu, C. M., & Wang, K. R. (2015). GIC due to storm sudden commencement in low-latitude high-voltage power network in China: Observation and simulation. *Space Weather*, 13, 643–655. <https://doi.org/10.1002/2015SW001263>
- Zois, I. P. (2013). Solar activity and transformer failures in the Greek national electric grid. *Journal of Space Weather and Space Climate*, 3. <https://doi.org/10.1051/swsc/2013055>